IEEE Access
Multidisciplinary | Rapid Review | Open Access Journal

Received September 4, 2019, accepted September 19, 2019, date of publication September 30, 2019,
date of current version October 24, 2019.

Digital Object Identifier 10.1109/ACCESS.2019.2944679

PDF-Euclidean Distance-Based Adaptive Waveform Selection for Maximizing Radar Practical Resolution

CHENGCHENG SI, BO PENG, AND XIANG LI
National University of Defense Technology, Changsha 410072, China

Corresponding author: Bo Peng (pengbo06@gmail.com)

This work was supported by the National Natural Science Foundation of China under Grant 61701510.

ABSTRACT This paper focuses on the issue of adaptive waveform selection to optimize the radar resolvability of closely located targets, which is significant in radar detection and estimation. The well-known ambiguity function-based radar resolution only takes transmitted waveform into consideration, which cannot reflect the achievable resolution of a real radar system. In this paper, we consider radar practical resolution based on a geometric metric, Euclidean Distance between probability density functions (PDF-ED), which is defined as square difference between the probability density functions of radar measurements. The PDF-ED takes the PDF's envelope curve into account and specifies the essential difference between the two PDFs in terms of information geometry. Thus the radar practical resolution based on this conveniently characterizes the effect of waveform parameter, target state and measurement model, etc. and offers a statistical way to assess radar sensing capability for a given application. Accordingly, an adaptive waveform selection criterion aiming to maximize the practical resolution is proposed. The experimental simulations verify its effectiveness in decreasing the probability of error when distinguishing two targets.

INDEX TERMS Adaptive waveform selection, PDF-Euclidean distance, radar practical resolution.

I. INTRODUCTION

The ability to distinguish multiple adjacent targets, usually represented by resolution, is of great importance for evaluating the performance of radar and other sensing systems. As a basic concept in radar signal processing, it has important applications in the fields of detection, tracking, imaging, etc [1], [2]. Usually, radar resolution is defined as the half power beam width (HPBW) of the radar response of the target in a certain dimension [3] such as range, velocity, etc.

Woodward originally proposed the ambiguity function of a signal [4], which can be regarded as the output of radar matched filter in the absence of noise [5]. The shape of the ambiguity function is strongly dependent on the waveform and specifies the shape of radar resolution cell [6]. This concept has been extended to fit different signal forms (e.g. narrow band [7], wide band [6]), measurement parameters (e.g. acceleration [5], azimuth [9]) and radar systems (e.g. monostatic radar, bistatic radar). Nevertheless, the resolution derived from ambiguity function just focuses on the intrinsic resolution, in other words, the potential resolution of the transmitted waveform. A waveform has the same intrinsic resolution in low and high signal-to-noise ratio (SNR) conditions, which is almost impossible in practice due to the presence of noise.

Based on ambiguity function, many waveform optimization methods are proposed to design waveforms with extremely narrow main lobe and extremely low side lobes so as to improve the resolvability of adjacent targets [10]–[12]. The majority of these methods also concentrate on the intrinsic resolution of waveforms while seldom algorithms consider waveform optimization enhancing practical resolution.

In recent years, adaptive waveform design has attracted much interest among scholars in many situations such as target detection [13] and tracking [14], [15], parameter estimation [16] and target recognition [17]. These algorithms greatly improve the performance of radar. Yet as a basic parameter of radar, the adaptive waveform design for optimizing radar resolution also needs researching. Based on the mutual information, Nijsure *et al.* propose a waveform optimization

The associate editor coordinating the review of this manuscript and approving it for publication was Yingsong Li.

algorithm for an adaptive multi-input-multi-output (MIMO) radar, which results in improved resolution as the increase of iterations [18], [19].

The stochastic character of measurement is introduced to the definition of practical resolution in order to describe the radar resolution performance more accurately. Due to the presence of noise, the radar measurement is characterized by a likelihood function of measurement parameters. Reference [20] introduces Fisher information metric to measure the distance between likelihood functions and defines the information resolution, which is a practical resolution providing a unified statistical measure for the capability of sensing devices for a given application. But the high computation complexity for Fisher information distance provides difficulty for practical applications. Reference [21] proposes a practical resolution based on Kullback-Leibler Divergence and develops an adaptive waveform design method to optimize radar practical resolution. This gives a new way for radar adaptive waveform design. However, the Kullback-Leibler Divergence, not satisfying the symmetry and triangle inequality properties, is not a true metric [22]. Furthermore, the value of the Kullback-Leibler Divergence makes no sense when the overlap of the two distributions is little.

The manifold is equivalent to the Euclidean space in local cases and hence it is reasonable to use the Euclidean metric as an approximation for the Fisher information distance, which can greatly simplify the calculation. This paper adopts Euclidean Distance between the probability density functions (PDF-ED) to specify the radar practical resolution. This metric considers the geometric shape and structure of the PDF and is therefore a more accurate and reliable way to measure the difficulty for distinguishing different PDFs than the methods that considers the mean only. Via using the PDF-ED, the practical resolution takes the statistical properties of measurement, i.e. waveform, noise, measurement model and the radar cross section (RCS) fluctuation of targets into account. Compared with the intrinsic resolution derived from ambiguity function, the PDF-ED-based resolution is more suitable for practical situations. Furthermore, we propose an adaptive waveform optimization method using the PDF-ED criterion to maximizing the resolvability of adjacent targets, by which the selected waveform behaves better than the fixed waveform in terms of resolution.

The paper is organized as follows. Section 2 introduces PDF-ED to represent radar resolution and the adaptive waveform selection algorithm maximizing the resolvability of targets is proposed in section 3. The simulation results in section 4 validate the effectiveness of the proposed algorithm both in static and dynamic scenarios. Finally, section 5 concludes the whole paper.

II. PDF-ED-BASED RADAR RESOLUTION

In this section, we first present how the PDF-ED-based radar resolution is proposed. Then a comparison is made between it and ambiguity function-based radar resolution.

A. MINIMUM PROBABILITY OF ERROR AND PDF-ED

In practice, radar measurements of targets, which are random variables contaminated by noise, follows a parameter-based likelihood function. We consider the following hypothesis testing problem

$$\begin{cases} H_1 : \mathbf{x} = \mathbf{s}_1 + \mathbf{w} \\ H_2 : \mathbf{x} = \mathbf{s}_2 + \mathbf{w} \end{cases} \tag{1}$$

Here, $\mathbf{x}$ is the radar measurement. $\mathbf{s}_1$ and $\mathbf{s}_2$ are two closely spaced target states i.e. delay, doppler-shift, etc. $\mathbf{w}$ is zero-mean gaussian white noise with variance σ^2. So under the two hypotheses, $\mathbf{x}$ obeys Gaussian distributions with mean $\mathbf{s}_1$ and $\mathbf{s}_2$ respectively. Usually, both the two testing errors (H_1 is decided when H_2 is true and H_2 is decided when H_1 is true) are unexpected. And the error probability is defined as

$$P_e = P\left(H_1; H_2\right) + P\left(H_2; H_1\right) \tag{2}$$

where $P(H_i; H_j)$ represents the probability that H_i is decided when H_j is true. We design the detector satisfying the minimum probability of error [23]

$$\frac{p\left(\mathbf{x}|H_1\right)}{p\left(\mathbf{x}|H_2\right)} \underset{H_2}{\overset{H_1}{\lessgtr}} \gamma = \frac{P\left(H_2\right)}{P\left(H_1\right)} \tag{3}$$

In the case that $\mathbf{s}_1$ and $\mathbf{s}_2$ have the same prior probability, the total probability of errors, according to multiple-signal hypothesis theory, is [23]

$$P_e = Q\left(\frac{1}{2}\sqrt{\frac{\|\mathbf{s}_1 - \mathbf{s}_2\|^2}{\sigma^2}}\right) \tag{4}$$

where $Q\left(x\right) = \int_x^{+\infty} \frac{1}{\sqrt{2\pi}} \exp\left(-\frac{t^2}{2}\right) dt$, and $\|\mathbf{s}_1 - \mathbf{s}_2\|$ is the distance between $\mathbf{s}_1$ and $\mathbf{s}_2$.

Equation (4) informs that the total probability of incorrect decisions, which describes how difficult to distinguish the two signals in an extent, is just negatively related to the distance between them. In terms of probability theory, $\mathbf{s}_1$ and $\mathbf{s}_2$ are the mean values of the two hypotheses. It is suggested that the difficulty to distinguish the two distributions is only related to their means.

However, the mean is not the only factor that influences the resolvability of the hypotheses. Variance also has impact on it. As depicted in Fig. 1, there are the PDFs of some range measurements. The farther away from the radar, the lower the SNR, the greater the impact of noise, the "chunkier" the PDF. It is shown that the overlap between target 3 and target 4 is much larger than that between target 1 and target 2. It is implied that with the expanding overlap, the two targets at a fixed distance apart tend to be unresolvable due to the dropping SNR. Thus, it is more reliable to consider the distance between two PDFs $\|p\left(\mathbf{x}|H_1\right) - p\left(\mathbf{x}|H_2\right)\|$ using likelihood methods to represent the difficulty to distinguish the two hypotheses. In this paper, we use the Euclidean metric to measure the distance between the PDFs. And in order to distinguish from the traditional Euclidean Distance $\|\mathbf{s}_1 - \mathbf{s}_2\|$, we call $\|p\left(\mathbf{x}|H_1\right) - p\left(\mathbf{x}|H_2\right)\|$ as PDF-ED.

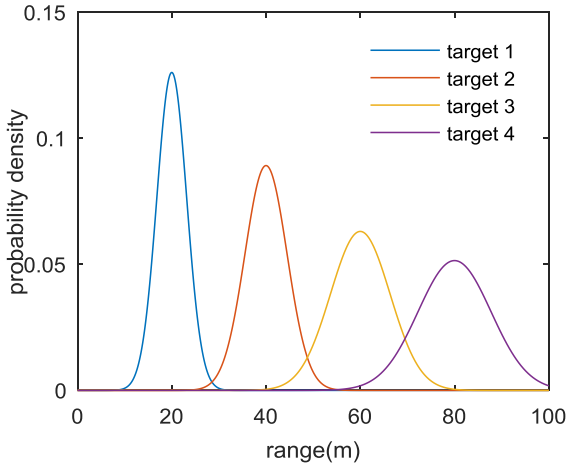

FIGURE 1. The likelihood functions of targets at fixed distance apart.

The PDF-ED between two PDFs $p_1(\mathbf{x})$ and $p_2(\mathbf{x})$ is obtained by integrating the squared difference over the whole PDF space.

$$\begin{aligned} e &= \|p_1(\mathbf{x}) - p_2(\mathbf{x})\| \\ &= \int_{-\infty}^{+\infty} [p_1(\mathbf{x}) - p_2(\mathbf{x})]^2 d\mathbf{x} \\ &= e_{11} + e_{22} - 2e_{12} \end{aligned} \tag{5}$$

where $e_{11} = \int_{-\infty}^{+\infty} [p_1(\mathbf{x})]^2 d\mathbf{x}$, $e_{22} = \int_{-\infty}^{+\infty} [p_2(\mathbf{x})]^2 d\mathbf{x}$, $e_{12} = \int_{-\infty}^{+\infty} p_1(\mathbf{x}) p_2(\mathbf{x}) d\mathbf{x}$. Especially, for two Gaussian distributions,

$$\begin{aligned} &\int_{-\infty}^{+\infty} N_1(\mathbf{x}; \boldsymbol{\mu}_1, \boldsymbol{\Sigma}_1) N_2(\mathbf{x}; \boldsymbol{\mu}_2, \boldsymbol{\Sigma}_2) d\mathbf{x} \\ &= \frac{1}{\prod_{n=1}^{N} \sqrt{\sigma_{1,n}^2 + \sigma_{2,n}^2}} \exp\left[-\frac{1}{2} \sum_{n=1}^{N} \frac{(\mu_{1,n} - \mu_{2,n})^2}{\sigma_{1,n}^2 + \sigma_{2,n}^2} \right] \end{aligned} \tag{6}$$

where $\boldsymbol{\mu}_i = [\mu_{i,1}, ..., \mu_{i,N}]$ $(i = 1,2)$ is the mean of Gaussian distribution and $\sigma_{i,n}$ $(i = 1,2; n = 1,...,N)$ is the nth diagonal element of its covariance matrix [24].

It is evident that PDF-ED is a true metric satisfying the nonnegativity, symmetry and triangle inequality properties, which accords with the physical background.

B. PDF-ED-BASED RADAR RESOLUTION

The following discussion presents how PDF-ED-based resolution is practical. It takes waveform parameters, SNR and radar measurement model into account and can be regarded as a statistical resolution from a statistical estimation view point. The radar measurement model is represented as

$$\mathbf{x} = h(\boldsymbol{\theta}) + \mathbf{w} \tag{7}$$

where $h(\cdot)$ describes the relationship between radar measurement $\mathbf{x} = [rv]^T$ and target state $\boldsymbol{\theta} = [\tau \ f_d]^T$. The parameters r, v, τ and f_d represent range, velocity, time delay and Doppler shift, respectively. The measurement noise $\mathbf{w}$ is approximated by a zero-mean Gaussian process with covariance $\boldsymbol{\Sigma}(\boldsymbol{\beta}, \boldsymbol{\theta})$, where $\boldsymbol{\beta}$ denotes the waveform parameter. It is assumed that the SNR is large enough so that the estimation achieves Cramer-Rao Lower Bound (CRLB). Hence the measurement noise covariance is approximated by the CRLB on the range and velocity estimation errors for the given waveform, which is calculated by [23]

$$\boldsymbol{\Sigma}(\boldsymbol{\beta}, \boldsymbol{\theta}) = \mathbf{J}\mathbf{I}^{-1}\mathbf{J}^T \tag{8}$$

Here, $\mathbf{J} = \mathrm{diag}\left(c/2, c/(2f_c)\right)$ is the Jacobian matrix and the Fisher information matrix is calculated by

$$\mathbf{I} = \begin{bmatrix} -\eta \dfrac{\partial^2 A(\tau, f_d)}{\partial \tau^2}\Big|_{\tau=0, f_d=0} & -\eta \dfrac{\partial^2 A(\tau, f_d)}{\partial \tau \partial f_d}\Big|_{\tau=0, f_d=0} \\ -\eta \dfrac{\partial^2 A(\tau, f_d)}{\partial f_d \partial \tau}\Big|_{\tau=0, f_d=0} & -\eta \dfrac{\partial^2 A(\tau, f_d)}{\partial f_d^2}\Big|_{\tau=0, f_d=0} \end{bmatrix} \tag{9}$$

where $A(\tau, f_d)$ is the ambiguity function of the given waveform and the SNR η is given by [25]

$$\eta = \frac{E_R}{N_0} = \frac{E_T G_t G_r c^2 \sigma}{(4\pi)^3 r^4 f_c^2 k T_s} \tag{10}$$

where E_R and E_T are the energy of the echo and the transmitted pulse respectively; $N_0 = kT_s$ is the power spectrum density (PSD) of the thermal noise at radar receiver; G_t and G_r denote the transmitting and receiving antenna gain respectively; σ represents the RCS of the target; f_c is the carrier frequency. And the speed of light $c = 3 \times 10^8$m/s, the Boltzmann constant $k = 1.38 \times 10^{-23}$J/K, the normal operating temperature $T_s = 290$ K. Noted that (10) considers an ideal situation where the transmitter directly sends its output to the antenna and there is no energy loss in the transmitter-target-receiver path.

Thus, for each state $\boldsymbol{\theta}$, the measurement $\mathbf{x}$ obeys a parameterized probability distribution $p(\mathbf{x}|\boldsymbol{\theta})$. Our work is to decide whether two target states $\boldsymbol{\theta}_1$ and $\boldsymbol{\theta}_2$ can be resolved according to the radar measurements.

From above discussion, our hypothesis testing problem is presented as

$$\begin{cases} H_1 : \mathbf{x} = h(\boldsymbol{\theta}_1) + \mathbf{w}_1 \sim N(h(\boldsymbol{\theta}_1), \boldsymbol{\Sigma}_1) \\ H_2 : \mathbf{x} = h(\boldsymbol{\theta}_2) + \mathbf{w}_2 \sim N(h(\boldsymbol{\theta}_2), \boldsymbol{\Sigma}_2) \end{cases} \tag{11}$$

The likelihood functions are

$$\begin{aligned} p(\mathbf{x}|H_1) = &\frac{1}{2\pi\sqrt{\det(\boldsymbol{\Sigma}_1)}} \\ &\cdot \exp\left(-\frac{1}{2} (\mathbf{x} - h(\boldsymbol{\theta}_1))^T \boldsymbol{\Sigma}_1^{-1} (\mathbf{x} - h(\boldsymbol{\theta}_1)) \right) \end{aligned} \tag{12}$$

$$\begin{aligned} p(\mathbf{x}|H_2) = &\frac{1}{2\pi\sqrt{\det(\boldsymbol{\Sigma}_2)}} \\ &\cdot \exp\left(-\frac{1}{2} (\mathbf{x} - h(\boldsymbol{\theta}_2))^T \boldsymbol{\Sigma}_2^{-1} (\mathbf{x} - h(\boldsymbol{\theta}_2)) \right) \end{aligned} \tag{13}$$

Based on [24], the PDF-ED between the two likelihood functions is

$$e\left(N\left(\mathbf{x};h\left(\boldsymbol{\theta}_1\right),\boldsymbol{\Sigma}_1\right)||N\left(\mathbf{x};h\left(\boldsymbol{\theta}_2\right),\boldsymbol{\Sigma}_2\right)\right) = \frac{1}{2\sqrt{\sigma_{1,1}^2\sigma_{1,2}^2}}+\frac{1}{2\sqrt{\sigma_{2,1}^2\sigma_{2,2}^2}}-\frac{2}{\sqrt{\sigma_{1,1}^2+\sigma_{2,1}^2}\sqrt{\sigma_{1,2}^2+\sigma_{2,2}^2}} \cdot \exp\left[-\frac{1}{2}\left(\frac{(r_1-r_0)^2}{\sigma_{1,1}^2+\sigma_{2,1}^2}+\frac{(v_1-v_0)^2}{\sigma_{1,2}^2+\sigma_{2,2}^2}\right)\right] \tag{14}$$

The larger the value of $e(N(\mathbf{x};h(\boldsymbol{\theta}_1),\Sigma_1)||N(\mathbf{x};h(\boldsymbol{\theta}_2),\boldsymbol{\Sigma}_2))$, the easier the two targets can be separated.

Therefore, the definition of PDF-ED-based resolution cells is given as: all equidistant points $\{\boldsymbol{\theta}'\}$ with identical PDF-ED from $\boldsymbol{\theta}_0$ form a practical resolution cell, i.e., for a given PDF-ED threshold, the practical resolution cell is the set $R=\left\{\boldsymbol{\theta}'|e\left(N\left(\mathbf{x};h\left(\boldsymbol{\theta}_0\right),\boldsymbol{\Sigma}_0\right)||N\left(\mathbf{x};h\left(\boldsymbol{\theta}'\right),\boldsymbol{\Sigma}'\right)\right)\leq e_T\right\}$, which is a section of the PDF-ED contour.

Based on this, the judging criterion (3) can be rewrote as

$$e\left(p\left(\mathbf{x}\right)||p\left(\mathbf{x}|H_1\right)\right)\underset{H_1}{\overset{H_0}{\lessgtr}}e\left(p\left(\mathbf{x}\right)||p\left(\mathbf{x}|H_2\right)\right) \tag{15}$$

where $p\left(\mathbf{x}\right)$ is the empirical PDF obtained from the radar measurements.

This PDF-ED-based resolution calculates the resolvability of targets in measurement domain, and corresponds to the waveform parameter, target state, and measurement model. Therefore, it is a more practical criterion for measuring the radar sensing performance. Also, for fluctuating targets, the RCS fluctuation also influences the uncertainty of radar measurements and is reflected in the PDFs. Thus the PDF-ED is also suitable for amplitude fluctuation situations. Besides, as the PDF-ED reflects the differences between the likelihood functions quantitatively, it promotes the radar resolvability of targets.

C. COMPARISON OF TRADITIONAL RESOLUTION AND PRACTICAL RESOLUTION

Traditional resolution cells, also called the intrinsic resolution cells, are the -3dB section of the normalized ambiguity function contour, i.e., $R_{AF}=\left\{\boldsymbol{\theta}'|\left|A\left(\boldsymbol{\theta}'\right)\right|\geq -3\text{dB}\right\}$, where $A\left(\boldsymbol{\theta}\right)$ is the normalized ambiguity function, which specifies the output of the matched filter in the absence of noise.

The following discussion compares intrinsic resolution and practical resolution based on PDF-ED in range-speed resolution with gaussian pulse of continuous wave (CW), whose corresponding noise covariance matrix is as follows [26], [27]:

$$s\left(t\right)=\left(\frac{1}{\pi\lambda^2}\right)^{\frac{1}{4}}e^{-\frac{t^2}{2\lambda^2}} \tag{16}$$

$$\boldsymbol{\Sigma}\left(\boldsymbol{\beta}\right)=\begin{bmatrix}\frac{c^2\lambda^2}{2\eta} & 0\\ 0 & \frac{c^2}{2\eta\lambda^2f_c^2}\end{bmatrix} \tag{17}$$

$$\boldsymbol{\beta}=\lambda \tag{18}$$

where λ denotes the duration of the Gaussian envelope.

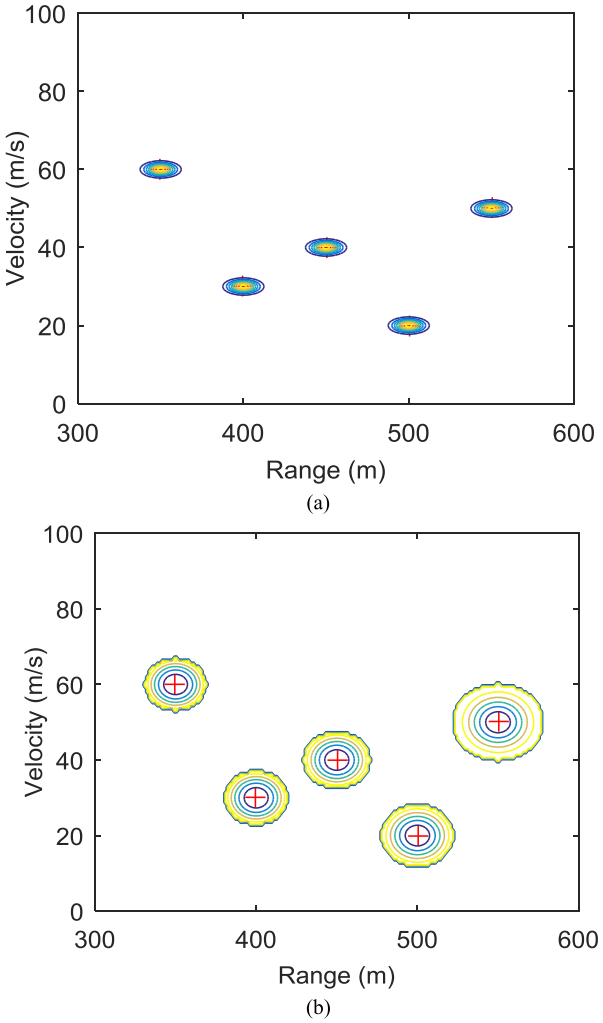

FIGURE 2. Differences between intrinsic resolution cells and practical resolution cells. (a) AF-based resolution cells of Gaussian pulse of CW (contour of AF); (b) PDF-ED-based resolution cells of Gaussian pulse of CW (contour of PDF-ED).

Fig. 2 presents the differences between intrinsic resolution and practical resolution of Gaussian pulse of CW (given $\lambda=1\mu$s, $f_c=5$ GHz). Five target states are given in the range-velocity plane where the resolution cells are obtained with their centers at the five crosses. Intrinsic resolution is only influenced by the waveform. Thus, as shown in Fig. 2(a), the resolution cell at each target state is the same, which reflects the potential resolution ability of the waveform. For practical resolution cell, it is related to the waveform and the target state, actually the SNR. Therefore, the shape and size of the resolution cell at each target are various, as seen in Fig. 2(b), indicating the resolution performance of the real radar system. Here, we set $e_T=30$.

Fig. 3 shows the improvement that PDF-ED brings to the signal processing performance. For convenience, we consider the resolution performance around $r=50$ km (given $\lambda=2\mu$s, $f_c=5$ GHz). Target A is static at 50 km and target B is moving around A. The measurements are generated from the two hypotheses alternately. Then we calculate the error

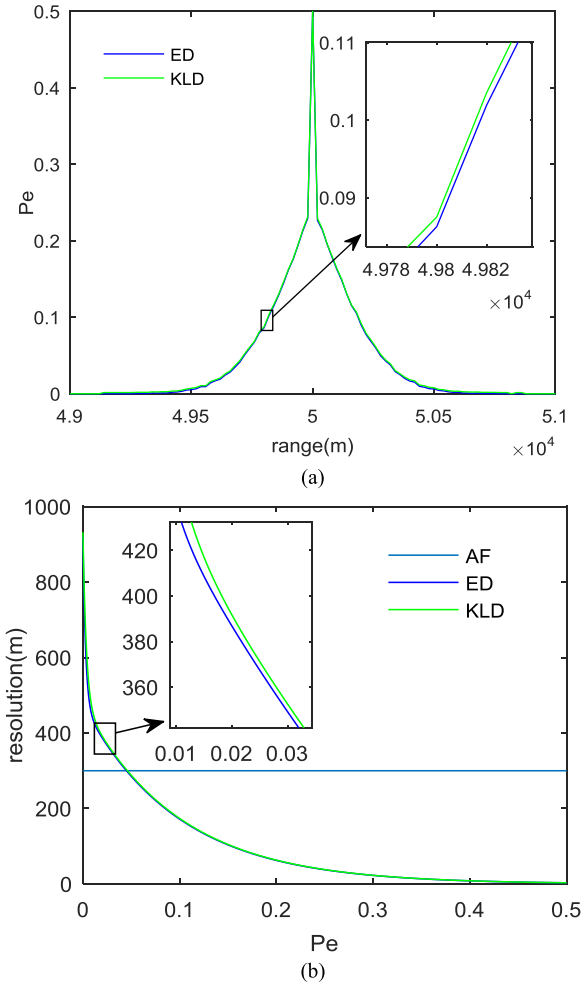

FIGURE 3. Illustration of practical range resolution based on PDF-ED. (a) error probability versus range; (b) comparison of resolutions versus error probability with different distance measures.

probability P_e of the detector (15) via 10^6 Monte Carlo simulations. Other simulation parameters for the radar system are listed in Table 1. It is clearly in Fig. 3(a) that the resolvability of the two targets deteriorates as target B approaching target A and they are completely unresolvable, i.e. $P_e = 0.5$ when they are at the same location. The values of corresponding to the Kullback-Leibler Divergence measure are also plotted for comparison. There is a slight drop of P_e by using PDF-ED metric. Based on this, we compare the practical resolutions versus the probability of error with different distance measures at detection range $r = 50$ km in Fig. 3(b). The practical range resolution cell is enlarged with the fall of the error probability owing to the requirement of a higher success rate. For the same error probability, the PDF-ED measure requires smaller resolution cell than the Kullback-Leibler Divergence measure. For a comparison, the intrinsic range resolution i.e. $\Delta r = c\lambda/2 = 300$m is also plotted. The comparison among the three types of resolutions indicates that adopting PDF-ED measure can adjust to the different precision requirements and promote the radar resolution performance in reducing the error probability.

TABLE 1. Simulation parameters for the radar.

Symbol	Quantity	Value
E_T	Transmitted energy	1 J
A	Target RCS	1 m2
G_t	Transmit-antenna-gain	20 dB
G_r	Receive-antenna-gain	20 dB

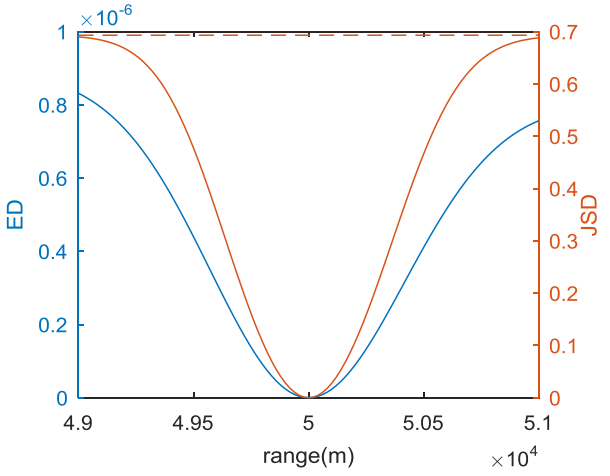

FIGURE 4. Comparison between Euclidean Distance and Jensen-Shannon Divergence versus range.

To illustrate the effectiveness of the PDF-ED, we also compare it to the Jensen-Shannon Divergence, which is a variant of Kullback-Leibler Divergence. As shown in Fig. 4, the Jensen-Shannon Divergence achieves its ceiling $\ln 2/2$ when the two targets are far enough apart. Then it becomes a constant and cannot reflect the difficulty distinguishing the two targets. By contrast, the PDF-ED does not have upper limit and does not have such trouble. Thus, the PDF-ED metric is more suitable for the radar resolution problem.

III. ADAPTIVE WAVEFORM SELECTION FOR MAXIMIZING PRACTICAL RESOLUTION

An adaptive waveform selection algorithm based on PDF-ED is proposed in this section, aiming to enhance the radar resolution performance in practice.

Provided two target state $\boldsymbol{\theta}_1$ and $\boldsymbol{\theta}_2$, the optimal waveform parameter $\boldsymbol{\beta}$ which maximizes the radar practical resolvability should satisfy

$$\max_{\boldsymbol{\beta}} \{e\left(p\left(\mathbf{x}|\boldsymbol{\theta}_1\right)||p\left(\mathbf{x}|\boldsymbol{\theta}_2\right)\right)\} \text{ st. } \boldsymbol{\beta} \in \Pi \tag{19}$$

where Π is the waveform parameter library and $e(p(\mathbf{x}|\boldsymbol{\theta}_1)||p(\mathbf{x}|\boldsymbol{\theta}_2))$ can be calculated by (14). For moving targets, namely the target states and the likelihood functions are dynamic, the PDF-ED between the two likelihood functions is a function of time. Therefore, the optimal waveform parameter can be selected adaptively at every instant to obtain the maximum PDF-ED and ultimately adapt to the environment changes.

The generic algorithm is used to solve the optimization problem, which is an adaptive global optimization search algorithm that simulates the genetic and evolutionary process of living organisms in the natural environment [28]. Each chromosome represents a waveform and each gene of the chromosome represents a parameter of the waveform. The fitness function is a measure to evaluate the quality of an individual, which is constructed as the objective function in (19), i.e.,

$$f = e\left(p\left(\mathbf{x}|\boldsymbol{\theta}_1\right)||p\left(\mathbf{x}|\boldsymbol{\theta}_2\right)\right) \tag{20}$$

Via mutation, crossover and positive natural selection, the fitness function is adjusted and reaches its peak after iterations. Then the corresponding waveform is the optimal.

To improve the iterative efficiency of the algorithm, the chromosome changing range is negatively correlated with its fitness value in the mutation operation. So the new gene x' after mutation is obtained by

$$x' = x \cdot \left(1 + r \cdot \left(\frac{f}{f_{best}}\right)^2\right) \tag{21}$$

where x is the original gene. r is a random number uniformly distributed between -1 and 1. f is the fitness value of the current individual and f_{best} is the highest fitness value in the current population.

In this paper, we focus on two types of waveforms, the Gaussian pulse of CW and the linear frequency modulation (LFM) pulse with Gaussian envelope. The noise covariance matrix of the former is (17) and that of the latter is as follows [26], [27]:

$$s\left(t\right) = \left(\frac{1}{\pi\lambda^2}\right)^{\frac{1}{4}} e^{-\frac{t^2}{2\lambda^2}+j2\pi bt^2} \tag{22}$$

$$\boldsymbol{\Sigma}\left(\boldsymbol{\beta}\right) = \begin{bmatrix} \frac{c^2\lambda^2}{2\eta} & -\frac{2\pi c^2 b\lambda^2}{\eta f_c} \\ -\frac{2\pi c^2 b\lambda^2}{\eta f_c} & \frac{c^2\left(1+16\pi^2 b^2\lambda^4\right)}{2\eta\lambda^2 f_c^2} \end{bmatrix} \tag{23}$$

$$\boldsymbol{\beta} = \left[\lambda\ b\right]^T \tag{24}$$

where λ and b parameterize the duration of the Gaussian envelope and the chirp rate of the frequency modulation respectively.

In order of comparison, the conventional ambiguity function-based waveform selection algorithm is also utilized, which selects waveforms by minimizing the trace of the noise covariance matrix. For Gaussian pulse of CW, the optimization problem is

$$\min_{\boldsymbol{\beta}} \left\{\frac{c^2\lambda^2}{2\eta} + \frac{c^2}{2\eta\lambda^2 f_c^2}\right\} \text{ st. } \boldsymbol{\beta} \in \Pi \tag{25}$$

(25) is equivalent to

$$\min_{\boldsymbol{\beta}} \left\{\lambda^2 + \frac{1}{\lambda^2 f_c^2}\right\} \text{ st. } \boldsymbol{\beta} \in \Pi \tag{26}$$

where the objective function and optimal result are independent of target states and SNR.

For LFM pulse with Gaussian envelope, the optimization problem for ambiguity function-based waveform selection is

$$\min_{\boldsymbol{\beta}} \left\{\frac{c^2\lambda^2}{2\eta} + \frac{c^2\left(1+16\pi^2 b^2\lambda^4\right)}{2\eta\lambda^2 f_c^2}\right\} \text{ st. } \boldsymbol{\beta} \in \Pi \tag{27}$$

(27) is equivalent to

$$\min_{\boldsymbol{\beta}} \left\{\lambda^2 + \frac{1+16\pi^2 b^2\lambda^4}{\lambda^2 f_c^2}\right\} \text{ st. } \boldsymbol{\beta} \in \Pi \tag{28}$$

where the objective function and optimal result are independent of target states and SNR.

Therefore, the waveform selection algorithm based on ambiguity function optimizes the fixed waveform and cannot select waveform adaptively to adjust to the change of target states. Our proposed algorithm addresses this problem and its performance is analyzed in the following section.

IV. NUMERICAL EXPERIMENTS

The proposed adaptive waveform selection method is applied both in stationary and dynamic scenes to choose optimal waveform parameter.

A. STATIONARY SCENE

The two static targets A and B are located at $r_A = 30$ km and $r_B = 30.5$ km along a radar line-of-sight respectively. For Gaussian pulse of CW, we take $\Pi = [1\mu s, 10\mu s]$ as the parameter library. The carrier frequency is $f_c = 10$ GHz. The waveform selected by the ambiguity function-based algorithm is for comparison. According to (7) and (17), the radar measurements of A and B are as follows:

$$\mathbf{x}|\boldsymbol{\theta}_A \sim N\left(\boldsymbol{\mu}_A, \boldsymbol{\Sigma}_A\right) = \left(\begin{bmatrix} r_A \\ v_A \end{bmatrix}, \begin{bmatrix} \frac{c^2\lambda^2}{2\eta_A} & 0 \\ 0 & \frac{c^2}{2\eta_A\lambda^2 f_c^2} \end{bmatrix}\right) \tag{29}$$

$$\mathbf{x}|\boldsymbol{\theta}_B \sim N\left(\boldsymbol{\mu}_B, \boldsymbol{\Sigma}_B\right) = \left(\begin{bmatrix} r_B \\ v_B \end{bmatrix}, \begin{bmatrix} \frac{c^2\lambda^2}{2\eta_B} & 0 \\ 0 & \frac{c^2}{2\eta_B\lambda^2 f_c^2} \end{bmatrix}\right) \tag{30}$$

Evidently $v_A = v_B = 0$. Taking (29) and (30) into (14), we have the objective function

$$e = \frac{f_c\left(\eta_A + \eta_B\right)}{c^2} - \frac{4f_c\eta_A\eta_B}{c^2\left(\eta_A + \eta_B\right)} \cdot \exp\left[-\frac{\left(r_A - r_B\right)^2\eta_A\eta_B}{c^2\lambda^2\left(\eta_A + \eta_B\right)}\right] \tag{31}$$

which is a monotonic decreasing function of λ. Therefore, the optimal waveform parameter in this scene is $\lambda_{opt} = 1\mu s$.

As for LFM pulse with Gaussian envelope, the parameters are selected where $\lambda \in [1\mu s, 10\mu s]$ and $b \in \left[10^{12}\text{Hz/s}, 10^{13}\text{Hz/s}\right]$. The waveform selected by the ambiguity function-based algorithm is for comparison. According

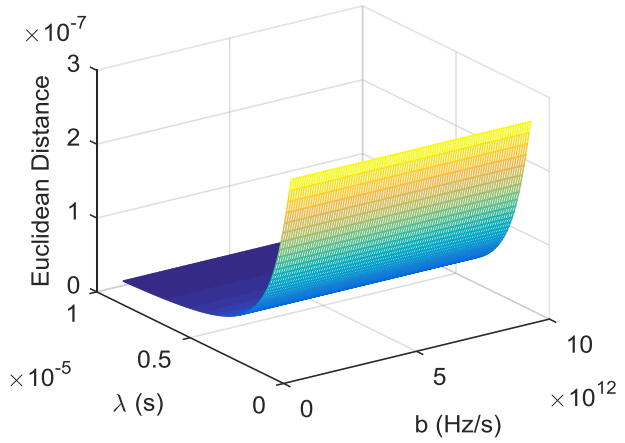

FIGURE 5. PDF-ED variation versus waveform parameters for LFM pulse with Gaussian envelope in the case of equal velocity.

to (7) and (23), the radar measurements of the two targets are

$$\mathbf{x}|\boldsymbol{\theta}_A \sim N\left(\boldsymbol{\mu}_A, \boldsymbol{\Sigma}_A\right) = \left(\begin{bmatrix} r_A \\ v_A \end{bmatrix}, \begin{bmatrix} \frac{c^2\lambda^2}{2\eta_A} & -\frac{2\pi c^2 b\lambda^2}{\eta_A f_c} \\ -\frac{2\pi c^2 b\lambda^2}{\eta_A f_c} & \frac{c^2\left(1+16\pi^2 b^2\lambda^4\right)}{2\eta_A\lambda^2 f_c^2} \end{bmatrix}\right) \tag{32}$$

$$\mathbf{x}|\boldsymbol{\theta}_B \sim N\left(\boldsymbol{\mu}_B, \boldsymbol{\Sigma}_B\right) = \left(\begin{bmatrix} r_B \\ v_B \end{bmatrix}, \begin{bmatrix} \frac{c^2\lambda^2}{2\eta_B} & -\frac{2\pi c^2 b\lambda^2}{\eta_B f_c} \\ -\frac{2\pi c^2 b\lambda^2}{\eta_B f_c} & \frac{c^2\left(1+16\pi^2 b^2\lambda^4\right)}{2\eta_B\lambda^2 f_c^2} \end{bmatrix}\right) \tag{33}$$

Taking (32) and (33) into (14), we obtain the objective function

$$e = \frac{f_c\left(\eta_A+\eta_B\right)}{c^2\sqrt{1+16\pi^2 b^2\lambda^4}} - \frac{4\eta_A\eta_B f_c}{c^2\left(\eta_A+\eta_B\right)\sqrt{1+16\pi^2 b^2\lambda^4}} \cdot \exp\left[-\frac{\left(r_A-r_B\right)^2\eta_A\eta_B}{c^2\lambda^2\left(\eta_A+\eta_B\right)}\right] \tag{34}$$

As suggested in Fig. 5, the PDF-ED in this case ascends with the decline of λ and has little relationship with. Hence, (34) is maximized by $\lambda_{opt} = 1\mu s$ and almost independent of b.

The error probability defined as (2) is utilized to access the performance of the proposed algorithm, which is calculated by 10^6 Monte Carlo simulations to improve the accuracy.

The probability of error in above cases is listed in Table 2. Compared with the ambiguity function-based algorithm, the proposed adaptive waveform method can lead to a considerable reduction of the error probability for both waveforms, which can be exploited to enhance the radar resolution. In parameter optimization, the proposed method is consisting with the waveform optimization algorithm based on Kullback-Leibler Divergence-based practical resolution.

TABLE 2. Error probability in stationary scene where $r_A = 30$ and $r_B = 30.5$.

	Gaussian pulse of CW	
	Adaptive	AF-fixed
Pe with ED	4.0550×10^{-4}	0.1051
Pe with KLD	4.2750×10^{-4}	0.1054
	LFM pulse with Gaussian envelope	
	Adaptive	AF-fixed
Pe with ED	3.9050×10^{-4}	0.0559
Pe with KLD	5.7050×10^{-4}	0.0565

TABLE 3. Error probability in stationary scene where $r_A = 40$ and $r_B = 40.5$.

	Gaussian pulse of CW	
	Adaptive	AF-fixed
Pe with ED	0.0172	0.1395
Pe with KLD	0.0175	0.1409
	LFM pulse with Gaussian envelope	
	Adaptive	AF-fixed
Pe with ED	0.0170	0.1102
Pe with KLD	0.0173	0.1118

However, the PDF-ED-based detector performs better in resolving the two targets and achieves a lower probability of error, because the PDF-ED specifies the difference between the two PDFs more accurately than the Kullback-Leibler Divergence.

To evaluate the robustness of the proposed method, another static scene is considered where target A and target B are located at $r_A = 40$ km and $r_B = 40.5$ km. The radar parameters are the same as the above. The simulation results are listed in Table 3. The proposed PDF-ED-based algorithm reduces the error probability significantly compared to the ambiguity function-based waveform design. The robustness of the algorithm in stationary scenes is also verified.

B. DYNAMIC SCENE

Two targets A and B are located at $r_A = 60.2$ km and $r_B = 60$ km along a radar line-of-sight at time instant $t = 0$ s respectively. They move towards the radar with velocity $v_A = 200$ m/s and $v_B = 100$ m/s. The carrier frequency is $f_c = 9$ GHz while the observation time is from 0 s to 4 s with $N = 100$ samples.

For Gaussian pulse of CW as model wave, the parameter is chosen from $\Pi = [1\mu s, 11\mu s]$, and the waveform optimized by the ambiguity function-based method is utilized for comparison. Similarly to the stationary scene, the objective function at discrete time instant $t[k]$ $(k = 0, 1, \ldots, N-1)$ is

$$e = \frac{f_c\left(\eta_A[k]+\eta_B[k]\right)}{c^2} - \frac{4f_c\eta_A[k]\eta_B[k]}{c^2\left(\eta_A[k]+\eta_B[k]\right)} \cdot \exp\left[-\frac{\left(r_A-r_B+\left(v_B-v_A\right)t[k]\right)^2\eta_A[k]\eta_B[k]}{c^2\lambda^2\left(\eta_A[k]+\eta_B[k]\right)}\right] \cdot \exp\left[-\frac{\left(v_B-v_A\right)^2\lambda^2 f_c^2\eta_A[k]\eta_B[k]}{c^2\left(\eta_A[k]+\eta_B[k]\right)}\right] \tag{35}$$

For simplicity, we rewrite the optimization problem as

$$\max_{\lambda\in\Pi}\left\{\frac{(r_A-r_B+(v_B-v_A)\,t\,[k])^2}{\lambda^2}+(v_B-v_A)^2\,\lambda^2 f_c^2\right\} \tag{36}$$

where the objective function is a concave function of λ and has the only minimum point, also the least point $\lambda_0 = \sqrt{\frac{|r_A-r_B+(v_B-v_A)t[k]|}{f_c|v_A-v_B|}}$. Thus, the optimal is either $\lambda_{\min}$ or $\lambda_{\max}$, which is illustrated in Fig. 6(a). At the very beginning, the two targets are far apart, and the PDF-ED is mainly dominated by range difference. The shorter time duration of signal is chosen to attain higher range resolution so as to distinguish them in range domain. When target A approaches target B, the difference in velocity dominates the PDF-ED. Increasing λ helps to improve the velocity resolution and then enlarge the PDF-ED. In the end, target A is departing from target B. The drop of λ is needed because range resolution is dominating the PDF-ED gradually.

Fig. 6(b) presents the trend of the probability of error during the whole process. As the velocity difference is constant, the PDF-ED first decreases and then increases with the change of the range between A and B. Thus the error probability tends to go up when A approaches B and go down when they depart. The error probability drops a little steeper than it rises because the increasing SNR helps to improve the resolvability of targets. It is obvious that the error probability of the adaptive selected waveform is much lower than that of the waveform based on the ambiguity function during the whole process, which infers the advantage of the proposed algorithm in radar resolution.

Furthermore, to compare the performance of the two criteria, the difference between the error probability under PDF-ED criterion and that under Kullback-Leibler Divergence criterion is plotted in Fig. 6(c). In most of the time, the former is smaller than the latter, indicating that using the PDF-ED-based detector helps to promote the resolvability of targets and achieve a lower error probability.

As for LFM pulse with Gaussian envelope, the parameters are selected where $\lambda \in [1\mu s, 11\mu s]$ and $b \in \left[10^{12}\text{Hz/s}, 10^{13}\text{Hz/s}\right]$. Similarly to the stationary scene, the objective function at instant $t[k]$ $(k = 0, 1, \ldots, N-1)$ is

$$\begin{aligned} e\,[k] = &\frac{f_c\,(\eta_A\,[k]+\eta_B\,[k])}{c^2\sqrt{1+16\pi^2b^2\lambda^4}} \\ &-\frac{4\eta_A\,[k]\,\eta_B\,[k]f_c}{c^2\,(\eta_A\,[k]+\eta_B\,[k])\,\sqrt{1+16\pi^2b^2\lambda^4}} \\ &\cdot\exp\left[-\frac{(r_A-r_B)^2\,\eta_A\,[k]\,\eta_B\,[k]}{c^2\lambda^2\,(\eta_A\,[k]+\eta_B\,[k])}\right] \\ &\cdot\exp\left[-\frac{(v_A-v_B)^2\,\lambda^2 f_c^2\eta_A\,[k]\,\eta_B\,[k]}{c^2\left(1+16\pi^2b^2\lambda^4\right)(\eta_A\,[k]+\eta_B\,[k])}\right] \end{aligned} \tag{37}$$

Via solving the optimization problem at each time instant, we acquire the dynamic optimal parameter shown in Fig. 7(a). The variation regularity of pulse width λ is similar with the case of Gaussian pulse of CW, while the chirp rate b keeps a low value to avoid velocity ambiguity. Here the proposed algorithm and the ambiguity function-based one

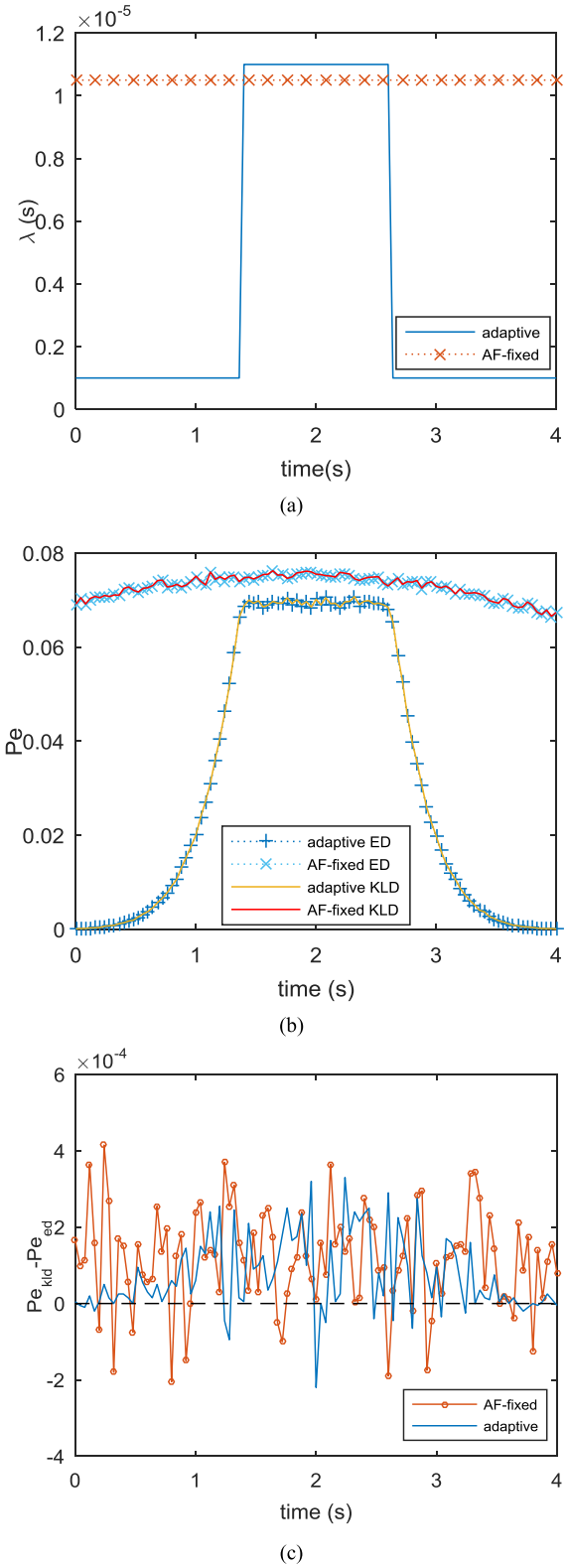

FIGURE 6. Adaptive waveform selection for Gaussian pulse of CW in dynamic scene. (a) waveform parameter versus time; (b) probability of error versus time; (c) the difference between the two criteria.

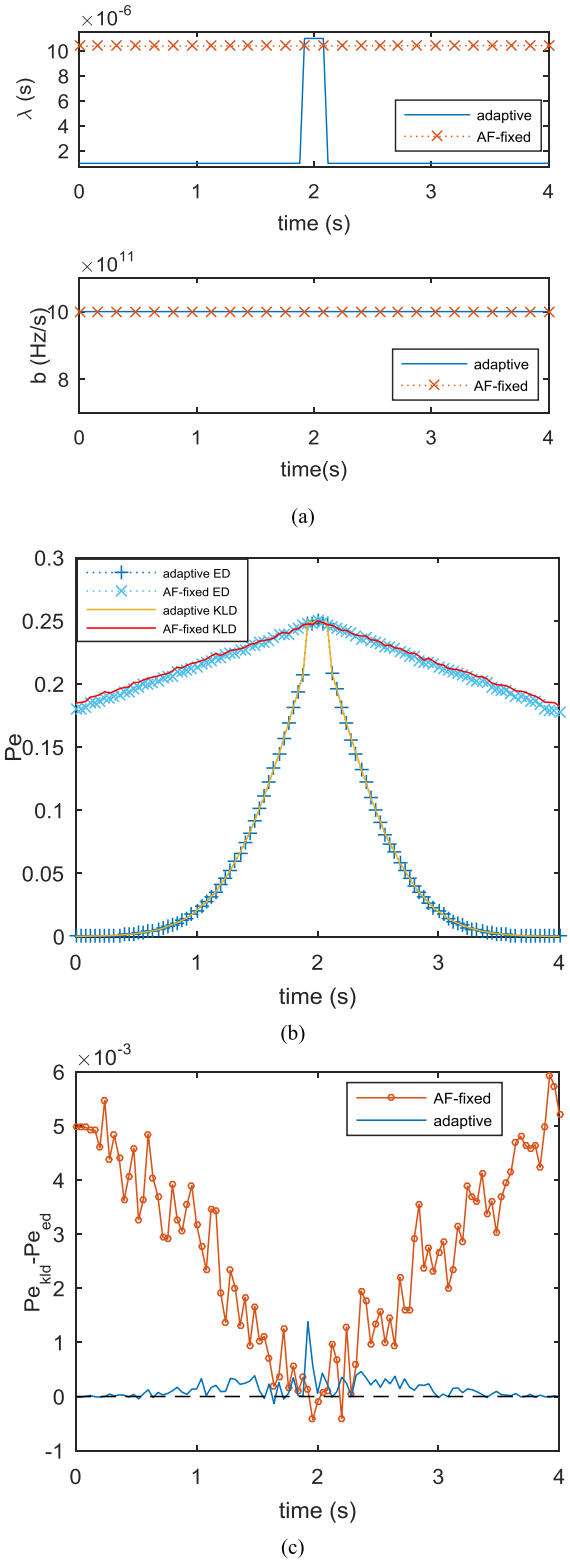

FIGURE 7. Adaptive waveform selection for LFM pulse with Gaussian envelope in dynamic scene. (a) waveform parameter versus time; (b) probability of error versus time; (c) the difference between the two criteria.

select the same chirp rate. The trend of error probability described in Fig. 7(b) is similar to the Gaussian pulse of CW case. It is suggested that the PDF-ED based algorithm can

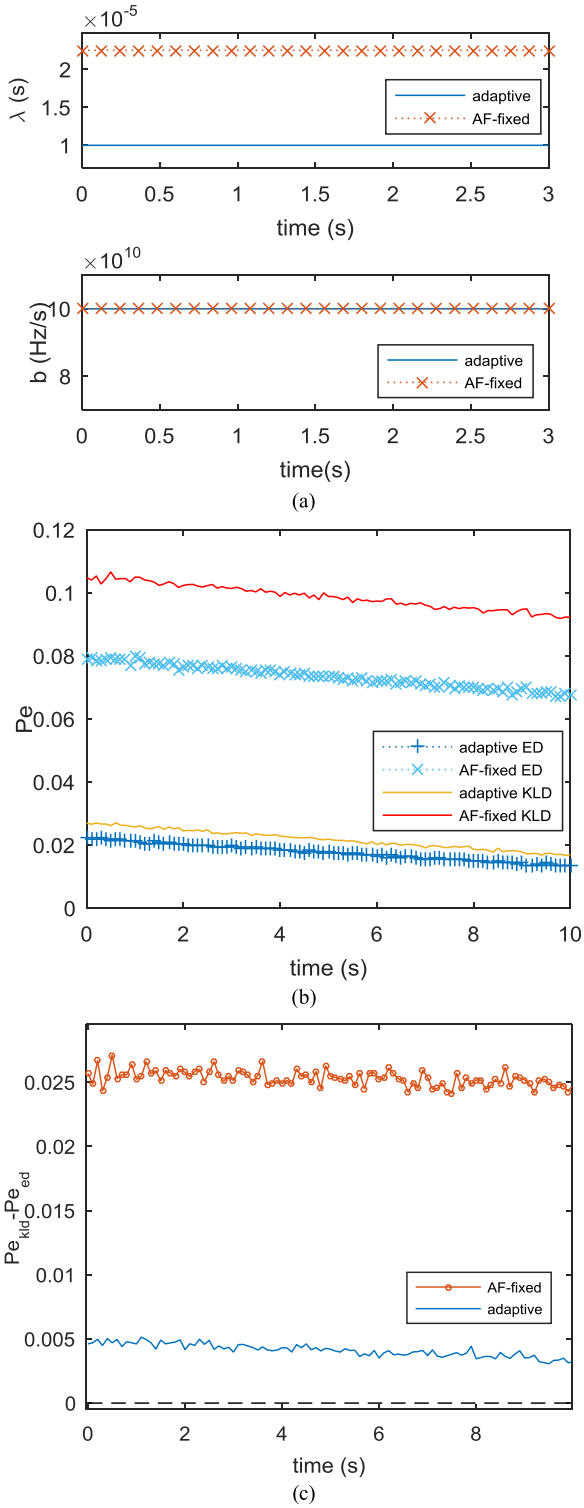

FIGURE 8. Simulation statistics for Scene 1. (a) waveform parameters; (b) error probability; (c) difference between the two criteria.

adjust the waveform parameter adaptively according to the change of target states and therefore improves the accuracy of radar resolution while the ambiguity function-based waveform selection method cannot. Besides, the error probability of the PDF-ED-based detector tend to be lower than that of the KLD-based one, which implies the slight advantage of the

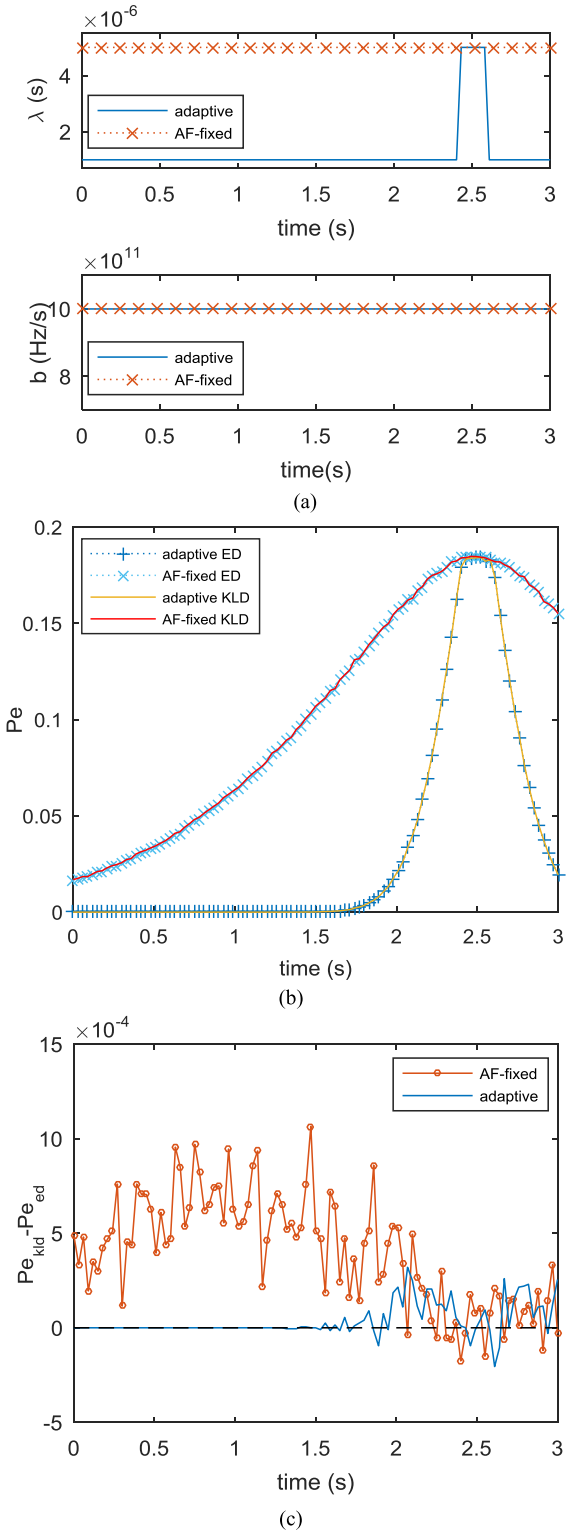

FIGURE 9. Simulation statistics for Scene 2. (a) waveform parameters; (b) error probability; (c) difference between the two criteria.

former in radar resolution. Therefore, the effectiveness of the proposed adaptive waveform selection method is validated.

The other two scenarios with moving targets are also considered to access the robustness of the algorithm. The simulation parameters are listed in Table 4.

TABLE 4. Simulation parameters for dynamic scenes.

		Scene 1	Scene 2
Initial position	r_A (km)	30.5	40.5
	r_B (km)	30	40
velocity	v_A (m/s)	200	200
	v_B (m/s)	200	0
Observation time	T (s)	0-10	0-3
Sample number	N	100	100
Carrier frequency	f_c (GHz)	2	2
Waveform library	λ (μs)	10-50	1-5
	b ($\times 10^{11}$ Hz/s)	1-5	10-50

Scene 1 is designed to evaluate the performance of the proposed algorithm in conditions where the targets are relatively static. The result is shown in Fig. 8. Because the velocity difference is zero, the optimization problem is the same as (34), the one for static scenes, where the PDF-ED falls down with the increase of λ and is almost unrelated with *b*. Thus the adaptive λ keeps a low value during the observation. Compared with the ambiguity function-based method, the proposed adaptive algorithm achieves a quite lower error probability, which can be applied to boost radar practical resolution.

The performance of the proposed algorithm in scenarios with moving and stationary targets is analyzed in Scene 2, where the optimization problem is similar to (37). The result is shown in Fig. 9. At around 2.5 s when the range difference is almost zero, the two algorithms select the same waveform. Hence their error probabilities are almost the same. In other time, the error probability of the proposed adaptive waveform is much lower than that of the ambiguity function-based one, which suggests the superiority of our method in radar practical resolution.

V. CONCLUSION

This paper proposes a novel approach to define radar practical resolvability based on PDF-ED. Compared with the traditional ambiguity function-based resolution, which only takes the waveform into account, the newly proposed resolution is a function of waveform parameter, target state and measurement model. As a result, it has a better environment adaptation and depresses the probability of incorrect decisions. The decision criterion based on this is suggested to have better performance in radar resolution. Consequently, we present an adaptive waveform selection algorithm maximizing the practical resolvability of a radar system. Simulation results verify the robustness and effectiveness of the algorithm.

ACKNOWLEDGMENT

The authors would like to thank the anonymous reviewers for their valuable comments on improving this article.

REFERENCES

[1] K. Liu, Y. Cheng, Y. Gao, X. Li, Y. Qin, and H. Wang, "Super-resolution radar imaging based on experimental OAM beams," *Appl. Phys. Lett.*, vol. 110, no. 16, Apr. 2017, Art. no. 164102.

[2] M. T. Lin, Y. Gao, P. Liu, and J. Liu, "Super-resolution orbital angular momentum based radar targets detection," *Electron. Lett.*, vol. 52, no. 13, pp. 1168–1170, Jun. 2016.
[3] D. K. Barton, P. C. Hamilton, S. A. Leonov, A. Leonov, *Radar Technology Encyclopedia*, Boston, MA, USA: Artech House, 1997.
[4] P. M. Woodward, *Probability and Information Theory with Applications to Radar*, London, U.K.: Pergamon Press, 1953.
[5] H. Urkowitz, C. A. Hauer, and J. F. Koval, "Generalized resolution in radar systems," *Proc. IRE*, vol. 50, no. 10, pp. 2093–2105, Oct. 1962.
[6] R. Niu, P. Willett, and Y. Bar-Shalom, "Tracking considerations in selection of radar waveform for range and range-rate measurements," *IEEE Trans. Aerosp. Electron. Syst.*, vol. 38, no. 2, pp. 467–487, Apr. 2002.
[7] L. Auslander and R. Tolimieri, "Characterizing the radar ambiguity functions," *IEEE Trans. Inf. Theory*, vol. 30, no. 6, pp. 832–836, Nov. 1984.
[8] L. G. Weiss, "Wavelets and wideband correlation processing," *IEEE Signal Process. Mag.*, vol. 11, no. 1, pp. 13–32, Jan. 1994.
[9] H. Zhao, Q. Fu, and J. Zhou, "The analysis of acceleration resolution and application for the radar signal," *Acta Electron. Sinica*, vol. 31, no. 6, pp. 958–960, 2003.
[10] M. G. M. Hussain, "Ambiguity functions for monostatic and bistatic radar systems using UWB throb signal," *IEEE Trans. Aerosp. Electron. Syst.*, vol. 47, no. 3, pp. 1710–1722, Jul. 2011.
[11] T. D. Bhatt, E. G. Rajan, and P. V. Rao, "Design of high-resolution radar waveforms for multi-radar and dense target environments," *IET Radar, Sonar Navigat.*, vol. 5, no. 7, pp. 716–725, Aug. 2011.
[12] F. Ghani, S. Rosli, A. Ghani, R. Ahmed, "Waveform design for improved range and Doppler resolution in radar," in *Proc. 3rd Int. Conf. Intell. Syst. Modelling Simulation*, Kota Kinabalu, Malaysia, Feb. 2012, pp. 247–251.
[13] Y. Wei, H. Meng, Y. Liu, and X. Wang, "Extended target recognition in cognitive radar networks," *Sensor*, vol. 10, no. 11, pp. 10181–10197,2010.
[14] N. H. Nguyen, K. Dogancay, and L. Davis, "Adaptive waveform selection for multistatic target tracking," *IEEE Trans. Aerosp. Electron. Syst.*, vol. 51, no. 1, pp. 688–701, Jan. 2015.
[15] N. H. Nguyen, K. Doğançay, L. Davis, "Adaptive waveform scheduling for target tracking in clutter by multistatic radar system," in *Proc. IEEE Int. Conf. Acoust., Speech Signal Process.*, Florence, Italy, May 2014, pp. 1449–1453.
[16] J. Wang, Y. Qin, H. Wang, and X. Li, "Dynamic waveform selection for manoeuvering target tracking in clutter," *IET Radar, Sonar Navigat.*, vol. 7, no. 7, pp. 815–825, Aug. 2013.
[17] M. Fan, D. Liao, X. Ding, X. Li, "Waveform design for target recognition on the background of clutter," in *Proc. 8th Eur. Radar Conf.*, Manchester, U.K., Oct. 2011, pp. 329–332.
[18] Y. Chen, Y. Nijsure, C. Yuen, Y. H. Chew, Z. Ding, and S. Boussakta, "Adaptive distributed MIMO radar waveform optimization based on mutual information," *IEEE Trans. Aerosp. Electron. Syst.*, vol. 49, no. 2, pp. 1374–1385, Apr. 2013.
[19] Y. A. Nijsure, "Cognitive radar network design and applications," M.S. thesis, School Elect. Electron. Eng., Newcastle Univ., Newcastle upon Tyne, U.K., May 2012.
[20] Y. Cheng, X. Wang, T. Caelli, X. Li, and B. Moran, "On information resolution of radar systems," *IEEE Trans. Aerosp. Electron. Syst.*, vol. 48, no. 4, pp. 3084–3102, Oct. 2012.
[21] L. Wang, H. Wang, Y. Cheng, Y. Qin, P. V. Brennan, "Adaptive waveform design for maximizing resolvability of targets," in *Proc. 18th Int. Conf. Digit. Signal Process.*, Fira, Greece, Jul. 2013, pp. 1–6.
[22] T. M. Cover, J. A. Thomas, *Elements of Information Theory*. Hoboken, NJ, USA: Wiley, 2012.
[23] S. M. Kay, *Fundamentals of Statistical Signal Processing, Volume II: Detection Theory*. Upper Saddle River, NJ, USA: Prentice-Hall, 1998.
[24] M. Helen and T. Virtanen, "Query by example of audio signals using Euclidean distance between Gaussian mixture models," in *Proc. IEEE Int. Conf. Acoust., Speech Signal Process.*, Honolulu, HI, USA, Apr. 2007, pp. 225–228.
[25] D. K. Barton, *Radar Equations for Modern Radar*, Boston, MA, USA: Artech House, 2012.
[26] L. Pallotta, "Covariance matrix estimation for radar applications," M.S. thesis, Dipartimento Ingegneria Elettricae delle Tecnol. dell'Inf., Univ. degli Studi Napoli Federico II, Naples, Italy, 2014.
[27] M. I. Skolnik, *Radar Handbook*. New York, NY, USA: McGraw-Hill, 2008.
[28] D. Liu and J. Shu, "A modified decision tree algorithm based on genetic algorithm for mobile user classification problem," *Sci. World J.*, vol. 2014, Feb. 2014, Art. no. 468324.

CHENGCHENG SI received the B.S. degree in electronic engineering from the National University of Defense Technology (NUDT), Changsha, China, in 2017, where she is currently pursuing the M.S.E.E. degree with the School of Electronic Science and Engineering. Her current research interests include radar signal processing and waveform design.

BO PENG received the B.S. degree in information engineering and the Ph.D. degree from the National University of Defense Technology (NUDT), Changsha, China, in 2008 and 2014, respectively, where he is currently a Lecturer with the School of Electronic Science. His current research interests include radar signal processing, micro-Doppler, and waveform design.

XIANG LI received the B.S. degree from Xidian University, Xi'an, China, in 1989, and the Ph.D. degree from the National University of Defense Technology (NUDT), Changsha, China, in 1998, where he is currently a Professor with the School of Electronic Science. His current research interests include radar signal processing, automation target recognition, and waveform design.